Area coverage of radial Lévy flights with periodic boundary conditions

Mahsa Vahabi,[1,2] Johannes H. P. Schulz,[1] Babak Shokri,[2,3] and Ralf Metzler[4,5]

[1]*Physics Department, Technical University of Munich, D-85747 Garching, Germany*
[2]*Department of Physics, Shahid Beheshti University, General Campus, Evin, Tehran 19839, Iran*
[3]*Laser-Plasma Research Institute, Shahid Beheshti University, General Campus, Evin, Tehran 19839, Iran*
[4]*Physics Department, University of Potsdam, D-14476 Potsdam-Golm, Germany*
[5]*Physics Department, Tampere University of Technology, FI-33101 Tampere, Finland*

We consider the area coverage of radial Lévy flights in a finite square area with periodic boundary conditions. From simulations we show how the fractal path dimension d_f and thus the degree of area coverage depends on the number of steps of the trajectory, the size of the area, and the resolution of the applied box counting algorithm. For sufficiently long trajectories and not too high resolution, the fractal dimension returned by the box counting method equals two, and in that sense the Lévy flight fully covers the area. Otherwise, the determined fractal dimension equals the stable index of the distribution of jump lengths of the Lévy flight. We provide mathematical expressions for the turnover between these two scaling regimes. As complementary methods to analyze confined Lévy flights we investigate fractional order moments of the position for which we also provide scaling arguments. Finally, we study the time evolution of the probability density function and the first passage time density of Lévy flights in a square area. Our findings are of interest for a general understanding of Lévy flights as well as for the analysis of recorded trajectories of animals searching for food or for human motion patterns.

I. INTRODUCTION

Lévy flights are Markovian random walk processes, in which the lengths of individual jumps are distributed according to a probability density $\lambda(x)$ of the asymptotic power-law form [1–4]

$$\lambda(x) \simeq \frac{\sigma^\alpha}{|x|^{1+\alpha}}, \quad 0 < \alpha < 2, \tag{1}$$

where σ is a scaling factor of physical dimension length $[\sigma] = $ cm. The resulting motion is spatially scale free due to the divergence of the jump length variance $\int x^2 \lambda(x) dx$. Lévy flights were popularized by Benoît Mandelbrot, who named them after his teacher, French mathematician Paul Lévy [5]. They have been mainly applied in the modeling of search processes, following the original idea by Klafter and Shlesinger [6]: While regular random walks in one or two dimensions have a high probability to return to already visited sites, Lévy flights combine a thorough local search with occasional long excursions, leading them to areas which likely have not been visited before. This strategy reduces unnecessary oversampling and thus represents an advantage to the searcher. Indeed, trajectories consistent with the long-tailed jump length pattern (1) have been reported for various animal species [7–11]. Even for molecular search, Lévy flights may emerge from the topology of the search space [12]. Due to a mix of modern means of transportation, also human motion behavior is characterized by travel lengths with a power-law distribution [13]. Long-tailed distributions of relocation lengths also change significantly the distribution pattern of diseases, as regular diffusion fronts are broken by, for instance, long-distance air travel, thus carrying the disease to completely disconnected places [14].

For land-based animals typical search processes are essentially two dimensional. In many cases we may also neglect the vertical dimension for birds or fishes, when the lateral extension is considerably larger than the maximal height and depth difference of the trajectory. Unbounded Lévy flights have a fractal dimension equal to the stable index $d_f = \alpha$. In an unbounded, two-dimensional search space, for a single Lévy flight trajectory therefore the area coverage is incomplete. Thus, some given area element in the search space may be hit by one single trajectory while it may be missed by another. In many cases, however, the search space is bounded. For instance, animals only search for food in their own territory, or the business travel patterns of an individual are confined to a certain country or continent. Apart from facing a bounded search space, it is often also relevant to have to consider finite time effects. For instance, a predator often does not cover its entire territory on a single day. It is therefore of interest to explore the time evolution of the area coverage of Lévy flights: How long does it take for the animal to efficiently explore its entire patch, or a disease to reach every little town in a country? How large is the area coverage at a given time? These questions of area coverage are directly connected with the ergodic properties of Lévy flights, that is, the reproducibility between individual realizations of the process.

In this paper, we consider radial Lévy flights in two-dimensional square areas with periodic boundary conditions. We investigate the time evolution of the effective fractal dimension of the flights for varying stable index α. As a complementary measure for the area coverage we analyze the time evolution of the mean squared displacement up to its saturation. Moreover, we analyze the time evolution of the probability density function and its moments. We also pursue the question on the typical time for the Lévy flight to first reach or pass the boundary of the square interval. The paper is organized as follows. In Sec. II, we briefly review the mathematical foundation of Lévy flights, before exploring the characterization of Lévy flights in Sec. III. Section IV summarizes the results.
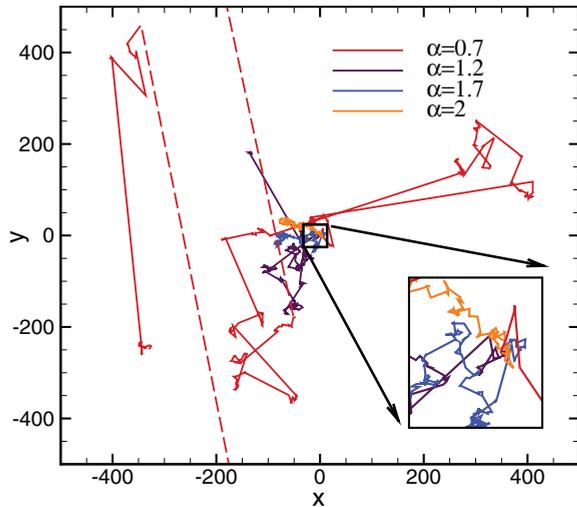
FIG. 1. (Color online) Trajectories of radial two-dimensional Lévy flights for different values of the stable exponent α, showing 400 steps each in a 1000×1000 box under periodic boundary conditions. The starting points for all trajectories were in the center of the square area. Note the significantly longer excursions for smaller values of α. The dashed line for the case $\alpha = 0.7$ depicts a jump across the periodic boundary. For all trajectories we chose $\sigma = \sqrt{2}$. The enlargement illustrates the self-similar nature of the Lévy flight trajectories.

II. LÉVY FLIGHTS

For jump length distributions of type (1), the variance $\langle x^2 \rangle = \int_{-\infty}^{\infty} x^2 \lambda(x) dx$ of jump lengths diverges, while fractional moments $\langle |x|^\delta \rangle$ of order $0 < \delta < \alpha$ exist [4]. The lack of scale $\langle x^2 \rangle$ carries over directly to the random motion itself and is responsible for several peculiar phenomena. Thus, the long-tailed nature of $\lambda(x)$ allows occasional, extremely long jumps to occur. This creates local clusters of the points of visitation along the trajectory, connected by long jumps. The clustering occurs on all scales ("clusters within clusters within clusters"), so that unvisited holes exist on all scales within the sample path. Consequently, Lévy flights have a fractal graph dimension $d_f = \alpha$ [2]. Figure 1 depicts typical sample trajectories of Lévy flights with a different stable index α. Note the distinct long jumps for smaller values of α. Remarkably, the discontinuous jumps on arbitrarily large scales induce a principal discrepancy between first passage and first arrival events. For instance, while their first passage behavior on a semi-infinite domain obeys the Sparre-Anderson universality [15,16], their first arrival behavior is significantly reduced with decreasing stable index α [15], as Lévy flights strongly overshoot a point target [16]. On finite domains the first passage behavior is also modified [17,18]. Another interesting effect is the occurrence of multimodal distributions for Lévy flights in the presence of steeper than harmonic potentials [19,20].

Lévy stable laws with a power-law asymptotic behavior (1) emerge as the limiting distribution for the sums of independent, identically distributed random variables with diverging variance, by virtue of the generalized central limit theorem [2,3,5,21]. In the symmetric case the characteristic function $\langle \exp(ikx) \rangle$ of a Lévy stable law is given by the

stretched Gaussian [2–5,21]

$$\lambda(k) \equiv \int_{-\infty}^{\infty} \lambda(x) e^{ikx} dx = \exp(-\sigma^\alpha |k|^\alpha), \qquad (2)$$

where, as mentioned, σ sets a typical length scale characteristic of the width of the characteristic function (2) and $\lambda(x)$ itself. For $0 < \alpha < 2$ the characteristic function (2) leads to the asymptotic power law (1), while in the limit $\alpha = 2$, we recover a Gaussian distribution for $\lambda(x)$ with finite moments of all orders. From the details of the microscopic jump length distribution, only the tail property (1) is directly passed on to the macroscopic displacements in the sense of the limiting transition of many summands.

Here, we consider two-dimensional, radial Lévy flights in square boxes of edge length $2a$, with periodic boundary conditions. This means that each time the particle crosses one edge of the box, it will enter from the opposite edge, as shown in Fig. 1. All Lévy flights start from the origin in the center of the square box. For each step in the two-dimensional trajectory we draw a flight distance r, whose distribution $\lambda(r)$ is identical to (1) and independently a flight direction θ. As we use the symmetric distribution with characteristic function (2) the "radius" r carries a sign, and we therefore choose the direction θ uniformly from the interval $[0, \pi]$. The projection of displacements onto the x axis is thus $r \cos(\theta)$. We call this a *radial*, two-dimensional Lévy flight. Such radial Lévy flights have been used to analyze search processes (see, e.g., Ref. [7]), and they appear to be a natural choice for an animal that controls radial distances during its motion. We note that radial Lévy flights are slightly different from two-dimensional, Cartesian Lévy flights defined in terms of two-dimensional characteristic functions $\exp(-[\sigma^*]^\alpha |\mathbf{k}|^\alpha)$ [22].

In what follows we calculate parameters such as the fractal dimension, spatial moments of the trajectories, the mean first passage time, and the probability density function of radial Lévy flights, in order to characterize their properties under periodic boundary conditions. We particularly focus on the area coverage of radial Lévy flights and its measurement from given recorded trajectories.

III. RESULTS AND DISCUSSION

A. Fractality of confined Lévy flights

The fractal dimension d_f indicates how completely a fractal object fills the available embedding space. While for mathematical fractals such as the von Koch snowflake or the Cantor set d_f equals the self-similarity dimension of the object, for random fractals d_f is defined in a statistical sense. That is, d_f is an average measure for the fractal, albeit the details of each realization will be different. Stochastic trajectories are one example for random fractals. Thus, the sample path of Brownian motion has a fractal dimension $d_f = 2$: It is completely space filling in two dimensions, but it is sparse in three dimensions, as reflected in its returning (Polyá) probability [2,23]. A Lévy flight with stable index $0 < \alpha < 2$ is already sparse in a two-dimensional embedding, and for $0 < \alpha < 1$ even in one dimension. A common way to determine the fractal dimension of random fractals is the box counting method [24], which we apply below.

TABLE I. Value of the stable index α of free, radial Lévy flights. We compare the input stable index α used to generate the sample trajectories and the output value for α as measured from the box counting analysis of the sample trajectories. The number of steps is an indication for the number of steps of the simulated Lévy flight (duration of the trajectory) necessary to determine α to reasonable accuracy. For $\alpha = 1.2$ we also include values for the output α for significantly shorter trajectories, demonstrating the tendency to undershoot the input α in such cases of insufficient statistics.

Input α	Number of steps	Output α
0.7	20 000	0.67 ± 0.11
1.2	400	0.91 ± 0.10
1.2	2000	1.07 ± 0.11
1.2	10 000	1.12 ± 0.09
1.2	50 000	1.13 ± 0.11
1.2	250 000	1.14 ± 0.11
1.7	100 000 000	1.62 ± 0.02

Specifically in our Lévy flight case we choose a suitable square area of size $(2a)^2$, in which we apply the box counting algorithm. For the bounded Lévy flights this square is defined by the periodic boundary conditions, while in the case of free Lévy flights it is chosen such that it extends beyond the fringe of the finite albeit long trajectory. In the box counting analysis we then draw on the original square a lattice with lattice constant $2a\epsilon$, where ϵ is a scaling factor of magnitude $0 < \epsilon \leqslant 1$. The number of boxes covering the original square with edge length $2a$ is then given by $1/\epsilon^2$. For each ϵ we count the number of boxes $N(\epsilon)$ containing at least one point of visitation of the trajectory. For an underlying fractal geometry and sufficiently small ϵ, a power-law relation of the form $N(\epsilon) \simeq \epsilon^{-d_f}$ is expected [24], and this box counting dimension d_f corresponds to the mathematical Hausdorff fractal dimension of the object [24].

To validate our method we first determine the fractal dimension of unbounded Lévy flights, for which the value $d_f = \alpha$ is expected. Our results are summarized in Table I. We find that the fractal dimension reproduces the stable index α quite reliably. However, the number of random walk steps (overall duration of the sample trajectories) necessary to obtain sufficient agreement between the input and output values for α increases dramatically with growing α. In Fig. 2 we show the box counting results for free Lévy flights with trajectories of 400–250 000 steps. As we can see the number of filled boxes $N(\epsilon)$ for shorter trajectories does not have a well-defined power-law region, while for an increasing number of steps the scaling region extends and allows us to determine a well-defined power-law exponent. If we determined local slopes in the log-log plot, it is clear that the obtained values will undershoot the expected limiting value $d_f = \alpha$. In Table I we also show the output value for the stable index α measured from the data shown in Fig. 2. This finite-size property needs to be taken into consideration when analyzing stochastic trajectories with the box counting method.

We consider here a particle motion in a *periodic* square box with edge length $2a$. Confinement of a Lévy flight will eventually alter its fractal properties significantly. Namely, due to reflections at the periodic boundaries, more and more points

$$a = \infty \text{ and } \alpha = 1.2$$
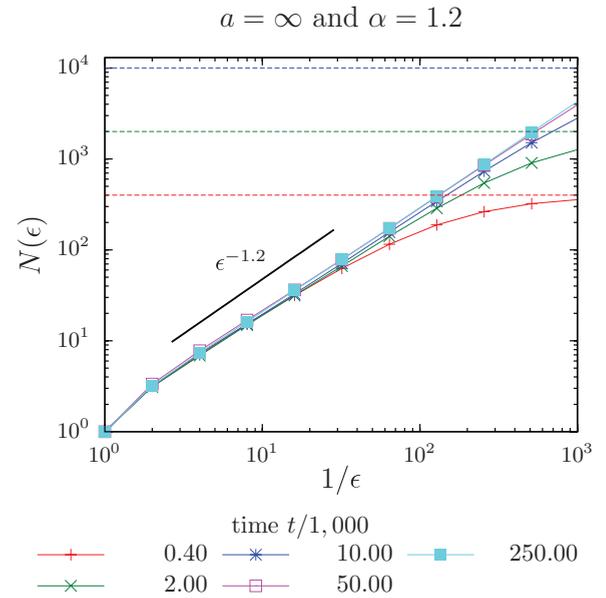
FIG. 2. (Color online) Box counting analysis of free Lévy flight trajectories of different duration t with stable index $\alpha = 1.2$ and $\sigma = \sqrt{2}$. If the analyzed sample trajectories are too short, no clear scaling window is returned. For an increasing number of steps of the trajectories the power-law behavior converges, and the box counting analysis eventually returns a sufficiently good value for the fractal dimension and thus the stable index of the trajectory. The horizontal lines indicate for the different trajectory durations the maximal number of filled boxes to which $N(\epsilon)$ saturates: Each box is filled with exactly one point of visitation of the trajectory such that a further increase in resolution does not increase the number of necessary boxes to cover the trajectory points. A straight line was fitted in the log-log plot to produce the results listed in Table I.

of visitation reach previously unvisited areas, and in the limit of extremely long trajectories we would expect a full area coverage, i.e., the box counting method should return a fractal dimension $d_f = 2$. In particular, in this limit each realization will be equivalent in the sense that all points of the area are visited, as long as we disregard the temporal sequence of the visitation.

Figures 3 and 4 show the results of box counting analyses for Lévy flights with stable indices $\alpha = 0.7$ and $\alpha = 1.2$. The results represent trajectories in boxes of varying size a (left panels) and at different numbers of steps per trajectory, t (right panels). In each realization the random walker starts in the center of the box. Consequently there exists a typical time scale $\tau \sim a^\alpha$ for the interaction with the confining boundaries (see below). For small times or large boxes ($t \ll \tau$), boundary effects are barely visible: The behavior is $N(\epsilon) \simeq \epsilon^{-\alpha}$ for the whole range of scale factors ϵ. Of course, we observe a deviation of this scaling when $\epsilon \to 1$: As long as we only measure at such a low resolution, obviously finite-size effects occur, in particular, at $\epsilon = 1$ the single box will always contain the trajectory, and $N(1) = 1$. Interestingly, the expected scaling for unconfined Lévy flights is already reached for $\epsilon = 1/8$. In contrast, once the random walker crosses the periodic boundaries many times ($t \gg \tau$), the behavior is more complex: A typical scaling factor ϵ_0 separates two fractal regimes. On large scales $\epsilon \gg \epsilon_0$, the trajectory
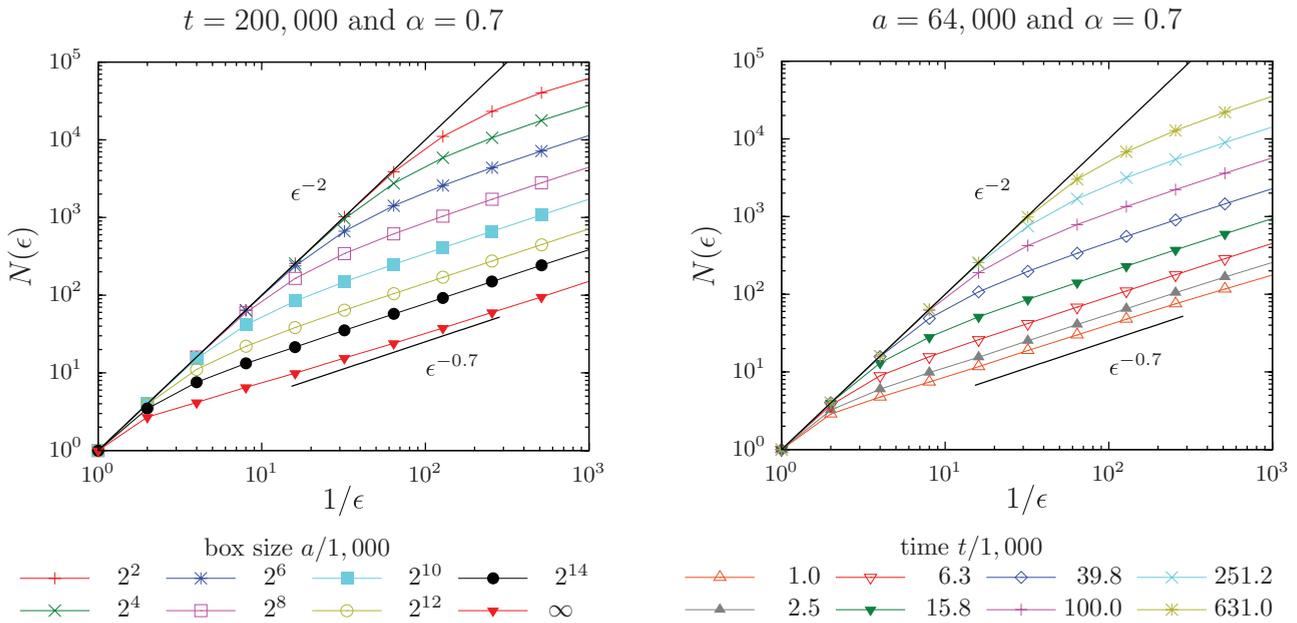
FIG. 3. (Color online) Results of the box counting method applied to radial Lévy flights with stable index $\alpha = 0.7$ and $\sigma = \sqrt{2}$ for various box sizes a (left) and evolution times t (right). Both panels show the number $N(\epsilon)$ of filled boxes at scale factor ϵ. Consistently for all cases we see a turnover from ϵ^{-2} scaling at large ϵ to $\epsilon^{-\alpha}$ scaling at small ϵ. See text.

shares its fractal characteristics with Brownian motion, i.e., $N(\epsilon) \simeq \epsilon^{-2}$. On small scales $\epsilon \ll \epsilon_0$, we identify the fractal scaling $N(\epsilon) \simeq \epsilon^{-\alpha}$. In what follows, we work out an intuitive reasoning for this curious bifractal behavior that is also useful for the practical determination of the fractal dimension of an empirical trajectory.

Imagine that we cut the full trajectory each time when the random walker crosses the boundary. Any of the resulting individual fragments of the trajectory could as well be part

of an unbounded Lévy flight, and therefore it represents a fractal with box counting dimension $d_f = \alpha$. Following this reasoning we can thus reinterpret the geometric structure in a periodic box as a stack of several fractal structures (fragments), each characterized by the same fractal dimension α. Due to the statistical nature of the stochastic trajectory, the points of visitation in individual fragments will differ, and each fragment lives in a separate virtual copy of the bounding box. Since
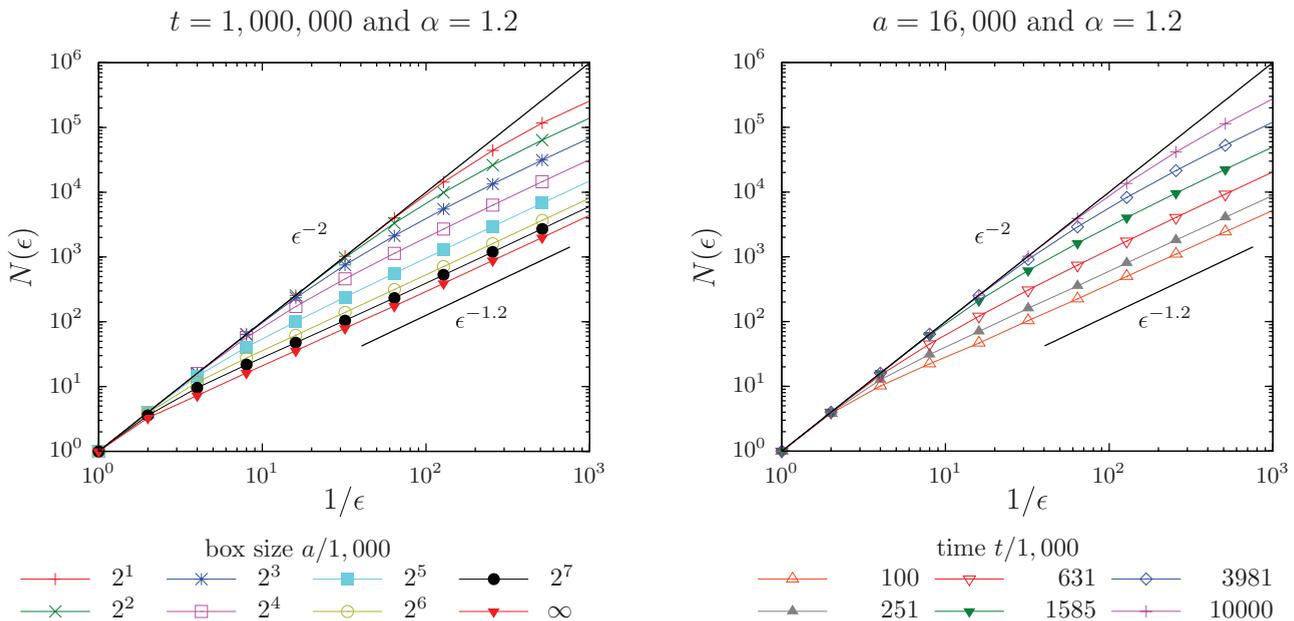
FIG. 4. (Color online) Results of the box counting method applied to radial Lévy flights with stable index $\alpha = 1.2$ and $\sigma = \sqrt{2}$ for various box sizes a (left) and evolution times t (right). Both panels show the number $N(\epsilon)$ of filled boxes at scale factor ϵ. Consistently for all cases we see a turnover from ϵ^{-2} scaling at large ϵ to $\epsilon^{-\alpha}$ scaling at small ϵ. See text.

Lévy flights are Markovian, the statistical properties of the fragments are independent from one fragment to the next.

Assume that the complete set of the points of visitation of a trajectory is contained in a total number n_c of copies (fragments) of our square box of size $(2a)^2$; n_c will be determined below. To obtain the fractal dimension, the bounding box is divided into $1/\epsilon^2$ smaller *local* boxes, and the number $N(\epsilon)$ of filled local boxes (i.e., containing at least one point of the trajectory) is counted. When scanning an individual box for trajectory points, the algorithm does not care which copy (fragment) of the system they originate from. Let p denote the probability to find some points of visitation in *any* of the copies of a local box within the stack. Since the copies are independent but share the same fractal dimension, p can be expressed in terms of $\bar{p}$, the probability to find some points in *one individual* copy of the local box,

$$p = 1 - (1 - \bar{p})^{n_c}. \tag{3}$$

Since the individual copies of our system are sets with a fractal dimension of α, on average we expect

$$\bar{p} = \frac{N(\epsilon)}{1/\epsilon^2} = \epsilon^{(2-\alpha)}. \tag{4}$$

We combine Eqs. (3) and (4) and find for the entire stack with all copies (fragments) of the trajectory the sought-after relation between the (ensemble averaged) number of filled boxes N and the scaling factor ϵ,

$$N(\epsilon) = p \cdot (1/\epsilon^2) = \epsilon^{-2}[1 - (1 - \epsilon^{(2-\alpha)})^{n_c}]. \tag{5}$$

It is worthwhile to check some limiting cases and compare them to known results as well as the numerical analysis presented in Figs. 3 and 4. For $\alpha = 2$, the measured fractal dimension should be $d_f = 2$, both in the absence and presence of the periodic boundaries. Indeed, Eq. (6) in this case yields $N(\epsilon) \sim \epsilon^{-2}$. Next, we consider unbounded Lévy flights by setting the number of copies (fragments) to $n_c = 1$. In this case, we find $N(\epsilon) = \epsilon^{-\alpha}$, as expected. Interestingly, for any $n_c > 1$, Eq. (5) exhibits a turnover from one scaling regime to another. Namely,

$$N(\epsilon) \simeq \begin{cases} \epsilon^{-2}, & \epsilon \gg \epsilon_0, \\ n_c \epsilon^{-\alpha}, & \epsilon \ll \epsilon_0, \end{cases} \tag{6}$$

leads to the area-filling result with exponent 2 or a scaling with the fractal graph dimension $d_f = \alpha$. The turnover occurs at some characteristic value ϵ_0 to be determined below. The predicted behavior from Eq. (6) explains the observations in Figs. 3 and 4.

We interpret the turnover behavior (6) of confined Lévy flights as follows. According to the above reasoning the random motion in a periodic box can be interpreted as a stack of fractal sets, each containing a fragment of an unbounded trajectory. These fractal sets are stochastically independent and share the same fractal dimension α. If the scaling factor ϵ is large (i.e., $\epsilon \sim 1$), the stack of trajectory fragments likely has points in all local boxes. Although in each copy (fragment) we may find some empty local boxes, they are unlikely to be in the same place for all copies. We therefore find a fractal dimension of 2 for the entire trajectory. However, once we increase the resolution (i.e., ϵ is smaller), the positions of filled

local boxes in each of the copies of the system become more and more specific. In this regime, it is unlikely to find filled local boxes at the same position for all copies. Thus, reflecting the independence of individual fragments, the total number of filled boxes is simply given by the number of copies n_c times the number of filled boxes per copy, $\epsilon^{-\alpha}$. From this analysis we see that it is important to choose the window of scaling factors ϵ sufficiently wide in order to be sure that an actual fractal object with $d_f < 2$ is not mistaken for a completely area-filling object ($d_f = 2$) due to finite-size effects.

We now address the question how the number of copies (fragments) n_c scales with the overall duration t of the trajectory and the size a of the square domain. We distinguish two regimes: When $t \ll \tau \simeq a^\alpha$, then any interaction of the random walker with the boundaries is negligible, and we are essentially facing an unbounded Lévy flight. In this limit, we observe that $n_c \approx 1$ and the fractal dimension is α. The opposite limit is $t \gg \tau$. In the interpretation of a stack of independent copies (fragments) of our system worked out above, this means that n_c becomes a large number. Then, Eq. (5) assumes the following asymptotic form,

$$N(\epsilon) \sim \epsilon^{-2} \left\{ 1 - \exp\left[-\left(\frac{\epsilon}{\epsilon_0} \right)^{(2-\alpha)} \right] \right\}, \tag{7}$$

with the characteristic scaling factor

$$\epsilon_0 = n_c^{1/(\alpha-2)}. \tag{8}$$

ϵ_0 separates the two fractal regimes in Eq. (6). In order to estimate how n_c (and consequently ϵ_0) relates to box size a and trajectory duration t, we note that τ is a typical time scale for boundary crossings. In particular, if $t \gg \tau$, we observe many boundary crossings and therefore expect $n_c \sim t/\tau \sim t/a^\alpha$. This yields the desired relation for ϵ_0,

$$\epsilon_0 \sim \frac{a^{\alpha/(2-\alpha)}}{t^{1/(2-\alpha)}}. \tag{9}$$

To compare these results with the numerical data, we introduce the rescaled quantities

$$\epsilon \to \xi \equiv \epsilon t^{1/(2-\alpha)} a^{-\alpha/(2-\alpha)},$$
$$N(\epsilon) \to g \equiv N(\epsilon) t^{-2/(2-\alpha)} a^{2\alpha/(2-\alpha)}. \tag{10}$$

With this choice Eq. (7) assumes the scaling form

$$g(\xi) \sim \xi^{-2} \left\{ 1 - \exp\left[-\left(\frac{\xi}{C_\alpha} \right)^{(2-\alpha)} \right] \right\}, \tag{11}$$

where $0 < C_\alpha$ is an appropriate scaling constant independent of the trajectory duration t and the domain size a. The rescaled version of the numerical data is displayed in Fig. 5. Indeed, the rescaled data points collapse neatly onto a single curve for a fixed value of α. The analytical form of Eq. (11) is also included in the plot. Due to the excellent collapse of data and analytical form, however, this curve is hardly visible. The parameter C_α was fitted for the individual trajectories, and the corresponding value is given in the figure legend.

A similar reasoning would apply in other embedding dimensions as well. For instance, adopting the above steps to a three-dimensional embedding, we expect that we see

	$\alpha = 0.7$			$\alpha = 1.2$	
	$\frac{t}{1,000}$	$\frac{a}{1,000}$		$\frac{t}{1,000}$	$\frac{a}{1,000}$
+	200.0	2^2	+	1000	2^1
×	200.0	2^4	×	1000	2^2
✳	200.0	2^6	✳	1000	2^3
□	200.0	2^8	□	1000	2^4
■	200.0	2^{10}	▽	631	2^4
▽	6.3	2^6	▼	1585	2^4
▼	15.8	2^6	◇	3981	2^4
◇	39.8	2^6	+	10000	2^4
+	100.0	2^6			
×	251.2	2^6			
✳	631.0	2^6			

Theory

—— $C_\alpha = 1.1$ —— $C_\alpha = 0.9$
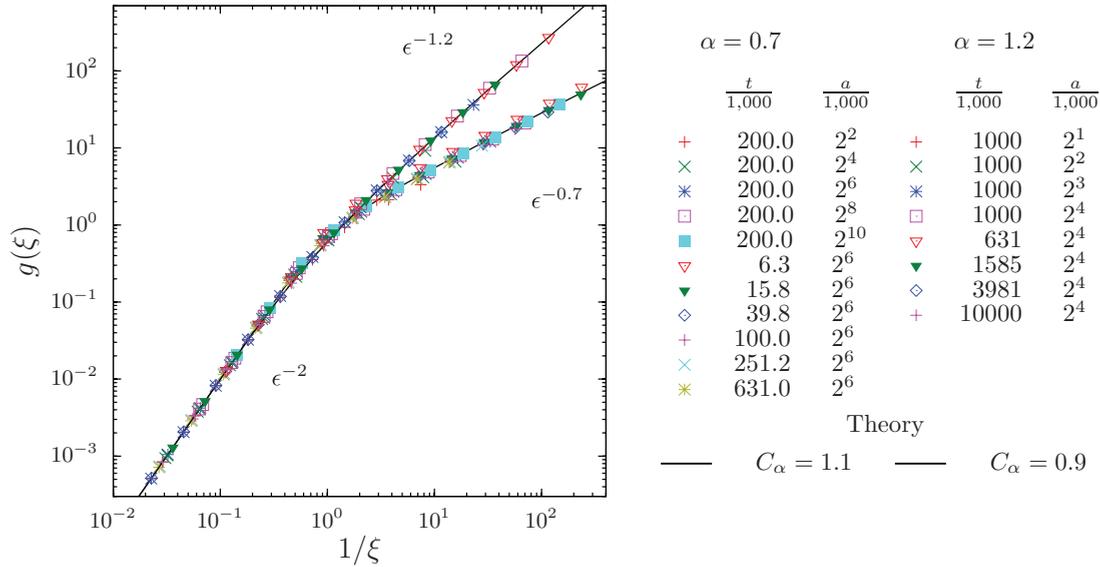
FIG. 5. (Color online) Rescaled results from Figs. 3 and 4 in terms of the scaling variable ξ and the scaling function $g(\xi)$ (see text for details). We chose those trajectories, for which the duration t exceeds the characteristic time scale τ. We see an excellent data collapse for all cases shown in the legend.

a turnover of the number of filled boxes as a function of the scale factor ϵ from $N(\epsilon) \sim \epsilon^{-3}$ to $N(\epsilon) \sim \epsilon^{-\alpha}$. The characteristic scale factor for the turnover will scale as $\epsilon_0 \sim a^{\alpha/(3-\alpha)}/t^{1/(3-\alpha)}$. Note that according to this observation even for ordinary Brownian motion we would observe a turnover from scaling exponent -3 to -2.

What do these results imply for an animal searching on a finite domain? We saw that on finer and finer scales ($\epsilon \gg \epsilon_0$) the trajectory assumes the fractal dimension $d_f = \alpha$ of a free Lévy flight. Only at a sufficiently coarse resolution ($\epsilon \ll \epsilon_0$) does a finite trajectory exhibit an apparent area-filling behavior, i.e., the scaling $N(\epsilon) \simeq \epsilon^{-2}$. For a searching animal using a Lévy flight search strategy this implies that in order to scan the entire area exhaustively during a single trajectory, it is imperative to have a reasonable field of vision, i.e., to be able to scan an area around each point of the trajectory. Even more efficient would be a constant scanning as discussed in Ref. [7], such that the scanned on-the-fly area represents a sausage. Without such provisions the scanning of the area by the Lévy flight remains sparse *a forteriori*. However, in a bounded system, the optimal scanning radius will actually depend on the system size and search time, and should be directly related to the spatial scale $a\epsilon_0$ beyond which the clustering nature of Lévy flight search strategies become relevant.

B. Moment analysis

We now turn to another quantity to characterize a Lévy flight trajectory on a finite domain with periodic boundary conditions and investigate the scaling behavior of spatial moments. To this end we consider the mean squared displacement $\langle x^2(t) \rangle$, for which we concentrate on the behavior along one of the axes of our square area. While this variance naturally diverges for a free Lévy flight or a Lévy flight in an harmonic external potential [4,20], it is already finite in steeper than harmonic external potentials [15]. In our square area the mean squared

displacement is thus a valid measure for the motion. Figure 6 shows the time dependence of the one-dimensional variance for different values of the stable index α. The saturation of the mean squared displacement is comparatively sharp, such that we can read off a typical time scale τ from Fig. 6 (see below). In the initial regime of effectively unbounded motion, $t \ll \tau$, all graphs depict a *linear* time dependence, independently of α. This highly contrasts the properties of unbounded Lévy flights, where x scales as $t^{1/\alpha}$ in the diffusion limit. In fact, from measuring the mean squared displacement alone, one could conclude to measure confined Brownian motion. Thus, the effect of the boundaries goes beyond ensuring the finiteness of the second moment. Interestingly, the boundaries also have
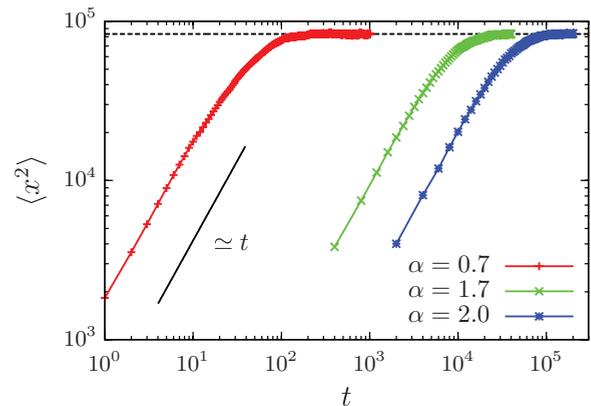
FIG. 6. (Color online) One-dimensional mean squared displacement of Lévy flights in a box with periodic boundary conditions and size 1000×1000 as function of time t, for different values of α. Here, 10 000 sample trajectories have been used for the ensemble average $\langle x^2(t) \rangle$. The horizontal black line represents the expected stationary value $a^2/3 = 83\,333$, where $a = 500$. Note that the early diffusion process is "normal" in the sense that $\langle x^2(t) \rangle$ grows linearly in time, despite the underlying scale-free jump distributions. See text.
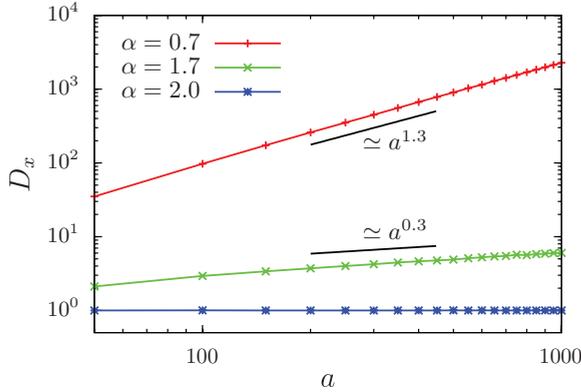
FIG. 7. (Color online) Diffusion constant vs box size. With the initial linear growth of the mean squared displacement, one can associate a diffusion constant $D_x = \langle x^2(t)\rangle/(2t)$. The latter has a power-law dependence on the edge length $2a$ of the box. Only for bounded Brownian motion, $\alpha = 2$, the (large) system size does not affect the initial diffusion parameters.

a distinct quantitative effect on the initial diffusion coefficient $D_x = \langle x^2(t)\rangle/(2t)$, as shown in Fig. 7: D_x depends on the size of the system. Enlarging the box increases the (finite) variance of individual jump lengths, thereby increasing D_x.

How can this behavior occur? To obtain the full picture we compute arbitrary moments of absolute displacements from our simulations. We generally find an initial power-law time dependence $\langle |x|^\delta(t)\rangle \simeq t^{e(\delta)}$ before the occurrence of saturation. More precisely, from the data for the scaling exponent $e(\delta)$ displayed in Fig. 8, we expect that in the asymptotic limit $1 \ll t \ll \tau$,

$$\langle |x|^\delta(t)\rangle \simeq \begin{cases} t^{\delta/\alpha}, & 0 < \alpha < 2 \text{ and } 0 < \delta < \alpha, \\ t, & 0 < \alpha < 2 \text{ and } \delta \geqslant \alpha, \\ t^{\delta/2}, & \alpha = 2 \text{ and } \delta > 0. \end{cases} \quad (12)$$

We note that this type of moment scaling is actually a familiar one in the theory of Lévy flights. It also occurs
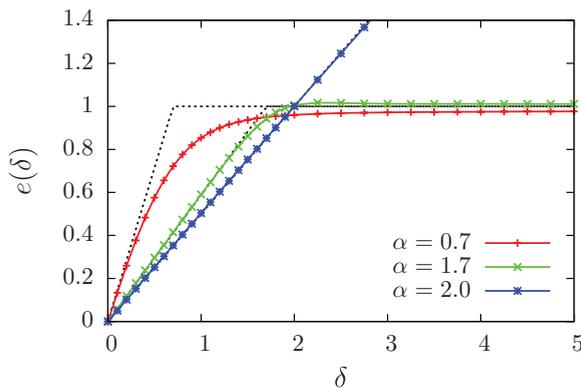
FIG. 8. (Color online) Scaling exponent $e(\delta)$ for moments $\langle |x|^\delta\rangle$ of arbitrary order $\delta > 0$. The exponent is obtained by a numerical fit to a power law, $\langle |x(t)|^\delta\rangle \simeq t^{e(\delta)}$. The theoretical prediction [black dotted lines, Eq. (12)] is valid only in the asymptotic limit $1 \ll t \ll \tau \simeq a^\alpha$. For this simulation, $2a = 10^5$, $t \in \{10, \ldots, 30\}$. The calculation of higher order moments exploits the far tails of the distribution, requiring a relatively large number (10^8) of trajectories.
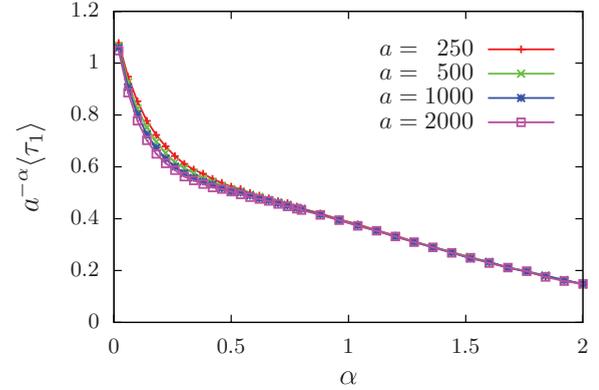
FIG. 9. (Color online) Rescaled mean first passage time of confined Lévy flights as function of the stable exponent α, for different box sizes. Here, $10^4 \ldots 10^5$ sample trajectories have been used for each data point.

when truncating the distribution (1) for the jump lengths at some fixed distance [25–27], or when considering the effects of a finite ensemble [28]. Roughly speaking, the truncation distance is analogous to the largest value drawn from a finite ensemble. In our system this role is played by the finite edge length of the box. In all such cases, the initial dynamics resemble an ordinary, unbounded Lévy flight, albeit with finite moments of type (12). In particular, we conclude that the second moment of bounded motion mimics normal diffusion, but the associated diffusion coefficient *must* depend on the system size parameter a. Conversely, at early times, moments with $0 < \delta < \alpha$ are adopted from the unbounded Lévy flight and are thus independent of a. At later times, all moments, independent of the fractional order δ, saturate at $\langle |x|^\delta(\infty)\rangle \simeq a^\delta$. The typical time scale for the interaction with the boundaries therefore scales as

$$\tau \simeq a^\alpha \quad \text{but also} \quad \tau \simeq a^2/(2D_x). \quad (13)$$

This necessarily implies that

$$D_x = D_x(a) \simeq a^{2-\alpha}. \quad (14)$$

The above relation is in nice agreement with our power-law fits in Fig. 7. The exponent also consistently coincides with the one found for the dependence on the truncation parameter in truncated but unbounded Lévy flights, as anticipated in Ref. [27].

C. Mean first passage time

As a further characteristic we briefly address the role of the mean first passage time $\langle \tau_1 \rangle$ of our confined Lévy flights to the boundary of the area. On a semi-infinite domain, Lévy flights show the universal Sparre-Anderson scaling $\simeq \tau_1^{-3/2}$ of the distribution of first passage times, so the mean first passage time $\langle \tau_1 \rangle$ diverges [15,16]. On our finite domain it converges and depends crucially on α. We determined the mean first passage time for Lévy flights with different values of α and for different box sizes ($a = 250$, 500, 1000, and 2000). From scaling arguments we would expect that the mean first passage time grows as $\langle \tau_1 \rangle \simeq a^\alpha$ as a function of the initial distance from the absorbing boundary [see Eq. (13)]. Figure 9 depicts

the rescaled mean first passage time $a^{-\alpha}\langle\tau_1\rangle$ as a function of α. We observe that the scaling relation holds provided that we can approximate the Lévy flight by a continuous diffusion process. Conversely, by choosing small values for a^α, we generate a random walker that escapes the box after only a few number of steps and the universal scaling (13) breaks down. From the monotonic nature of the graphs we conjecture that, for certain fixed parameters σ and a, one may find an optimal value for the stable index α which minimizes the mean first passage time.

We note that the analogous first passage time problem in one dimension has been treated analytically and numerically [29,30]. A generalization to our two-dimensional problem, however, is not straightforward: Although we fix the scale $\sigma = \sqrt{2}$ for individual jump distances r, displacements are still affected by random jump directions θ. One may argue that effectively the scale of displacements along the x, y, or radial coordinate is *not* fixed, but has a nontrivial relation to the tail parameter α. Consequently, such considerations raise the general question of how to appropriately fix a jump length scale for variable stable exponents in multidimensional Lévy flights.

D. Probability density function

Finally, we examine the probability density function of the process. Figure 10 shows the time evolution of the unidirectional probability density function $P(x,t)$ for Lévy flights with stable indices $\alpha = 0.7$ and 1.7. For comparison we also present graphs for Brownian motion, $\alpha = 2$. Starting with the sharp initial condition $P_0(x) = \lim_{t\to 0} P(x,t) = \delta(x)$, the probability density function successively broadens until it reaches equidistribution, $P_{st}(x) = 1/(2a)$. We observe that the specific characteristics of the different cases $0 < \alpha < 1$, $1 < \alpha < 2$, and $\alpha = 2$ remain discernible up to relatively long times. Thus up to some 10% of the overall simulation time, it is still possible to distinguish the basic shapes of the probability density functions for these cases. The overall simulation time needed to reach saturation is, however, dramatically different, as already observed in the labels shown in Fig. 10. This figure also demonstrates how fitting to a stable law, Eq. (2), yields an approximation of α. The fits in this figure show excellent agreement with simulation data.

Thus, from fitting probability density functions alone we could conjecture that the initial dynamics of the searcher starting far off the edges of the box is essentially unaffected by boundary conditions: At small times, the spatial distribution can be approximated by the stable law from an unbounded Lévy flight. However, the effect of boundaries is known to be highly nonlocal if the random walk is governed by long-tailed jump statistics (1). Due to the non-negligible probability for extremely long excursions, the searcher probes the nature of the boundaries from the very start of its motion. For example, this leads to modifications on the associated diffusion equations [31,32]. Figure 11 highlights the specific tail properties of the early-time distribution. Despite the almost perfect fit quality of stable distributions along virtually the whole search space, there are considerable deviations in the far tails near the boundaries. In particular, the distinct heavy-tail
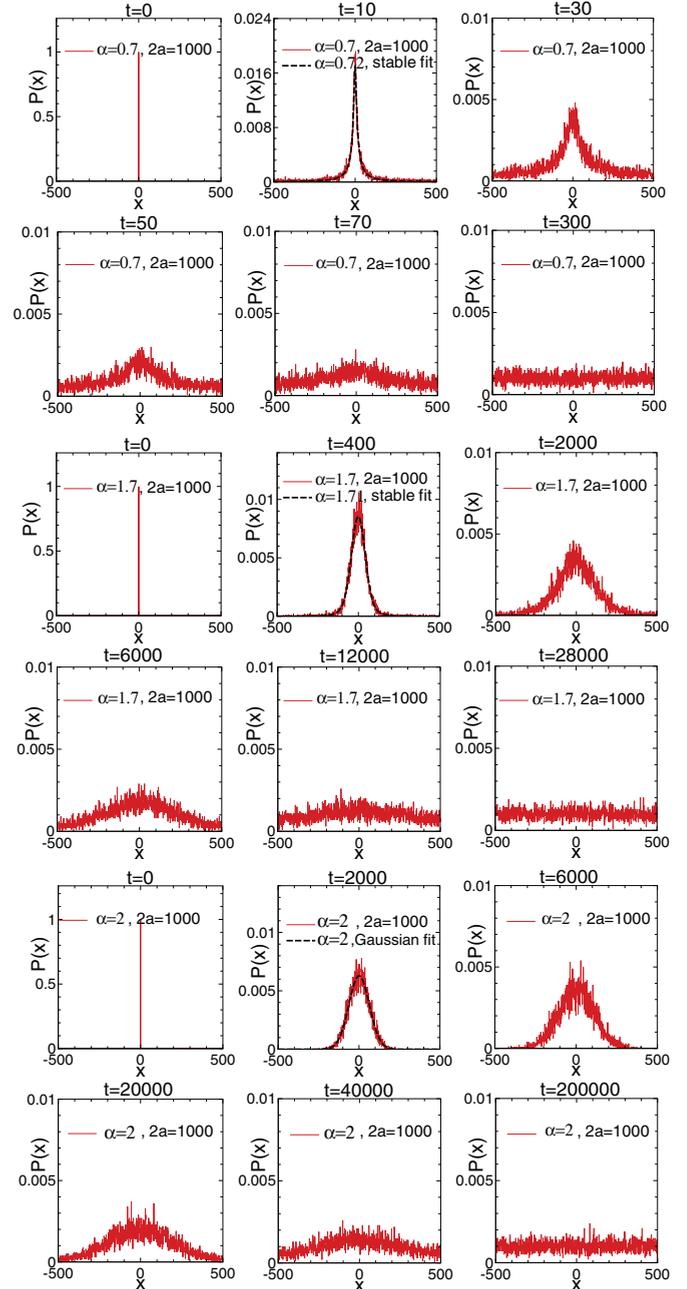
FIG. 10. (Color online) Time evolution of the unidirectional probability distribution function $P(x,t)$ of confined Lévy flights with $\alpha = 0.7$ and 1.7, as well as Brownian motion with $\alpha = 2$ in a box of edge length $2a = 1000$, for $\sigma = \sqrt{2}$. In each case 10 000 sample trajectories were used to create an individual curve for $P(x,t)$. Fits (dashed black lines) correspond to stable distributions as in Eq. (2).

property, Eq. (1), is already lost at this early stage of the random walk.

IV. CONCLUSIONS

Area coverage of stochastic processes is an important criterion for the efficiency of search or spreading processes. Here we investigated the time evolution of the area coverage in finite territories of Lévy flights. As measures we used the fractal dimension and moments of displacements of the
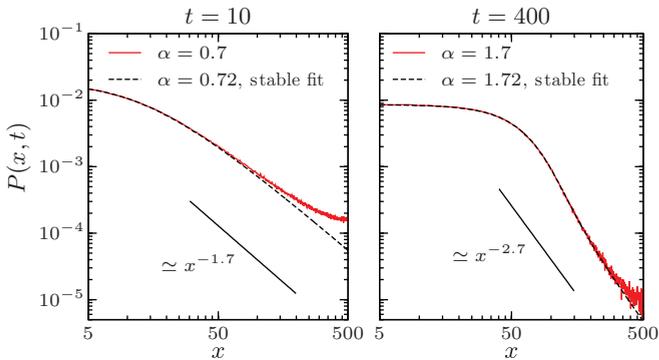
FIG. 11. (Color online) Tail analysis for the probability distribution function $P(x,t)$ of confined Lévy flights at an early stage of the random walk. The stable fits (dashed black curve) were performed for the same time instants as in Fig. 10, but a larger number of 3×10^6 of random walks were needed to produce precise tail data (continuous red curve).

Lévy flight. Consistently, we found that both quantities show a distinct saturation behavior, such that a clear time scale can be determined for reaching full area coverage. However, this time scale crucially depends on the value of the stable index α: When α approaches the limiting value two, this time scale increases significantly. As expected, smaller values for α, allowing for longer jump lengths, effect more efficient area coverage and thus search efficiency. In general, the number of steps necessary to reach full area coverage is relatively large. Thus searchers using this type of strategy will likely not be able to achieve absolute certainty to find a given target randomly. A field of vision, as introduced in the search literature, will abate this problem and render Lévy flights a very efficient search strategy.

As shown in our detailed analysis, interesting turnover behaviors come into play when we want to determine the fractal dimension of a stochastic trajectory. Thus, when the resolution in the box counting approach is too coarse, we will always recover full area coverage and thus an apparent fractal dimension of 2. Care has therefore to be taken to choose appropriate analysis windows. Concurrently, one needs to be aware of the subtlety of the scaling of spatial moments with time: For fractional moments whose order is at least equal to the stable index, we obtain a linear scaling with time, and the stable index α does not come into play. Only when the order of the moment is smaller than α do we obtain a typical scaling of free Lévy flights.

The analysis of the area coverage is completed with the study of the equilibration behavior of the probability density function of the process, allowing one to distinguish different domains of the stable index α (smaller or larger than one) up to relatively long times. Moreover, the mean first passage time

τ_1 scales with the index α and the system size approximately in the scaling fashion $\langle \tau_1 \rangle \simeq a^\alpha$.

From the data analysis point of view, we find that studying one single type of the above measures is usually not enough to identify a given motion as a bounded Lévy flight. The fractal dimension does have a characteristic behavior for long-tailed jump lengths, but quite extensive data is necessary to achieve reliable results from a box counting algorithm. Although fitting the spatial distributions by stable laws might agree nicely at the early stages of the process, their characteristic heavy tails are quickly reshaped by interactions with the boundaries. While the mean squared displacement indicates normal diffusion, the associated diffusion constant turns out to depend on the system size and lower order moments indicate superdiffusion. Finally, an analysis based on first passage times only yields decisive results if data on a variety of system sizes is available. Usually a combination of these complementary methods is necessary to determine the Lévy flight nature of a given process.

Finally, let us briefly address the ergodicity of the process. Ergodicity of stochastic processes has recently received considerable interest, following the possibility to record single trajectories of molecules or small tracers in biological matter or animals and human motion patterns, and to determine the expectation values of physical observables from time averages [33]. In an ergodic process, we expect that the time average of a physical observable becomes representative for the system and equal to the corresponding ensemble average at sufficiently long (infinite) times [34]. This holds true for Brownian motion as well as anomalous diffusion with Gaussian but power-law correlated noise described by the fractional Langevin equation or fractional Brownian motion [35–37]. However, for anomalous diffusion processes characterized by diverging time scales for the interjump waiting times, time averages remain random even for infinitely long trajectories, and time averaged observables behave differently from their ensemble analogs [33, 35,38], as also observed experimentally [39,40]. So what can be said about the ergodicity of Lévy flights? Unconfined Lévy flights in two dimensions (and generally when α is smaller than the embedding dimension) are nonergodic in the sense that they do not fully cover the area even at arbitrarily long times. Thus, for instance, the expectation of the outcome to find the particle in the first quadrant of the area will remain a random quantity [41]. Sufficiently long, confined Lévy flights, in contrast, are ergodic, as in the above sense they cover the full accessible area and each realization leads to the same result [42].

[1] B. B. Mandelbrot, *The Fractal Geometry of Nature* (Freeman, New York, 1983).

[2] B. D. Hughes, *Random Walks and Random Environments, Vol. 1: Random Walks* (Oxford University Press, Oxford, UK, 1995).

[3] J.-P. Bouchaud and A. Georges, Phys. Rep. **195**, 127 (1990).

[4] R. Metzler and J. Klafter, Phys. Rep. **339**, 1 (2000); J. Phys. A **37**, R161 (2004).

[5] P. Lévy, *Calcul des probabilités* (Gauthier-Villars, Paris, 1925); *Théorie de l' addition des variables aléatoires* (Gauthier-Villars, Paris, 1954).

[6] M. F. Shlesinger and J. Klafter, in *On Growth and Form*, edited by H. E. Stanley and N. Ostrowsky (Nijhoff, Amsterdam, 1986).

[7] G. M. Viswanathan *et al.*, Nature (London) **401**, 911 (1999); **381**, 413 (1996).

[8] G. Ramos-Fernandez, J. L. Mateos, O. Miramontes, G. Cocho, H. Larralde, and B. Ayala-Orozco, Behav. Ecol. Sociobiol. **55**, 223 (2004).

[9] D. W. Sims *et al.*, Nature (London) **451**, 1098 (2008); **465**, 1066 (2010).

[10] R. Nathan *et al.*, Proc. Natl. Acad. Sci. USA **105**, 19052 (2008).

[11] F. Bartumeus, J. Catalan, U. L. Fulco, M. L. Lyra, and G. M. Viswanathan, Phys. Rev. Lett. **88**, 097901 (2002).

[12] M. A. Lomholt, T. Ambjörnsson, and R. Metzler, Phys. Rev. Lett. **95**, 260603 (2005).

[13] D. Brockmann, L. Hufnagel, and T. Geisel, Nature (London) **439**, 462 (2006); M. C. González, C. A. Hidalgo, and A.-L. Barabási, *ibid.* **453**, 779 (2008).

[14] L. Hufnagel, D. Brockmann, and T. Geisel, Proc. Natl. Acad. Sci. USA **101**, 15124 (2004).

[15] A. V. Chechkin, R. Metzler, V. Yu. Gonchar, J. Klafter, and L. V. Tanatarov, J. Phys. A **36**, L537 (2003).

[16] T. Koren, M. A. Lomholt, A. V. Chechkin, J. Klafter, and R. Metzler, Phys. Rev. Lett. **99**, 160602 (2007).

[17] B. Dybiec, E. Gudowska-Nowak, and P. Hänggi, Phys. Rev. E **73**, 046104 (2006).

[18] S. Condamin, O. Bénichou, and M. Moreau, Phys. Rev. E **75**, 021111 (2007).

[19] A. V. Chechkin, V. Y. Gonchar, J. Klafter, R. Metzler, and L. V. Tanatarov, J. Stat. Phys. **115**, 1505 (2004); A. V. Chechkin, J. Klafter, V. Yu. Gonchar, R. Metzler, and L. V. Tanatarov, Phys. Rev. E **67**, 010102(R) (2003).

[20] S. Jespersen, R. Metzler, and H. C. Fogedby, Phys. Rev. E **59**, 2736 (1999).

[21] B. V. Gnedenko and A. N. Kolmogorov, *Limit Distributions for Sums of Random Variables* (Addison-Wesley, Reading, MA, 1954).

[22] A. V. Chechkin, V. Yu. Gonchar, and M. Szydlowski, Phys. Plasmas **9**, 78 (2002).

[23] In one dimension, the fractal dimension of a Brownian walk is one, however, its similarity dimension or mass dimension is two.

[24] K. Falconer, *Fractal Geometry: Mathematical Foundations and Applications* (Wiley, Chichester, UK, 1990).

[25] R. N. Mantegna and H. E. Stanley, Phys. Rev. Lett. **73**, 2946 (1994).

[26] I. Koponen, Phys. Rev. E **52**, 1197 (1995).

[27] H. Nakao, Phys. Lett. A **266**, 282 (2000).

[28] A. V. Chechkin and V. Y. Gonchar, Chaos, Solitons & Fractals **11**, 2379 (2000).

[29] A. Zoia, A. Rosso, and M. Kardar, Phys. Rev. E **76**, 021116 (2007).

[30] S. V. Buldyrev, S. Havlin, A. Ya. Kazakov, M. G. E. da Luz, E. P. Raposo, H. E. Stanley, and G. M. Viswanathan, Phys. Rev. E **64**, 041108 (2001).

[31] N. Krepysheva, L. Di Pietro, and M.-C. Néel, Phys. Rev. E **73**, 021104 (2006).

[32] B. Baeumer and M. M. Meerschaert, J. Comput. Appl. Math. **233**, 2438 (2010).

[33] E. Barkai, Y. Garini, and R. Metzler, Phys. Today **65**(8), 29 (2012).

[34] S. Burov, R. Metzler, and E. Barkai, Proc. Natl. Acad. Sci. USA **107**, 13228 (2010).

[35] S. Burov, J.-H. Jeon, R. Metzler, and E. Barkai, Phys. Chem. Chem. Phys. **13**, 1800 (2011).

[36] W. Deng and E. Barkai, Phys. Rev. E **79**, 011112 (2009).

[37] J. H. Jeon, H. Martinez-Seara Monne, M. Javanainen, and R. Metzler, Phys. Rev. Lett. **109**, 188103 (2012).

[38] Y. He, S. Burov, R. Metzler, and E. Barkai, Phys. Rev. Lett. **101**, 058101 (2008).

[39] A. V. Weigel *et al.*, Proc. Nat. Acad. Sci. USA **108**, 6438 (2011).

[40] J. H. Jeon, V. Tejedor, S. Burov, E. Barkai, C. Selhuber-Unkel, K. Berg-Sorensen, L. Oddershede, and R. Metzler, Phys. Rev. Lett. **106**, 048103 (2011).

[41] Compare the interesting discussion of nonergodic behavior in the presence of power-law statistics with diverging moments in optical lattices: E. Lutz, Phys. Rev. Lett. **93**, 190602 (2004).

[42] See the mathematical discussion in M. Magdziarz and A. Weron, Ann. Phys. **326**, 2431 (2011).